UNIVERSITY OF CALIFORNIA SAN DIEGO

Scalable thin film evaporator using capillary and osmotic pressure

A Thesis submitted in partial satisfaction of the requirements
for the degree Master of Science

in

Engineering sciences (Mechanical engineering)

by

Haowen Zhang

The committee in charge:

Professor Renkun Chen, Chair
Professor Jinhye Bae
Professor Shengqiang Cai

2023

The Thesis of Haowen Zhang is approved, and it is acceptable in quality and form for publication on microfilm and electronically.

University of California San Diego

2023

TABLE OF CONTENTS

THESIS APPROVAL PAGE.....iii

TABLE OF CONTENTS.....iv

LIST OF FIGURES.....v

LIST OF TABLES.....vi

ACKNOWLEDGEMENTS.....vii

ABSTRACT OF THE THESIS.....viii

CHAPTER 1: INTRODUCTION.....1

CHAPTER 2:THIN FILM EVAPORATION ON GLASS FIBER MEMBRANE.....5

CHAPTER 3:FEASIBILITY OF USING HYDROGEL IN EVAPORATOR WICK.....16

CHAPTER 4:SUMMARY AND FUTURE WORK.....24

REFERENCES.....27

LIST OF FIGURES

Figure 2.1 SEM image of glass fiber membrane after Pt sputtering……..……...…5

Figure 2.2 Schematics of sample preparation procedure...……..…6

Figure 2.3 TCR calibration curve of the Pt layer.....……..……7

Figure 2.4 Schematic and photos of evaporation set up.……..……8

Figure 2.5 Schematic of experimental setup..……...……9

Figure 2.6 Circuit diagram of evaporation set up.……...…..…10

Figure 2.7 Heat flux as a function of temperature……...……13

Figure 2.8 Effective heat transfer coefficient as a function of heat flux…...……...……14

Figure 3.1 Schematic and photo of permeability set up……...……...16

Figure 3.2 Schematic of hydrogel evaporation problem...……..……17

Figure 3.3 PSA max heat flux as a function of thickness……18

Figure 3.4 PEGDA max heat flux as a function of thickness..……19

Figure 3.5 Procedure of making hydrogel coated evaporator...……...…20

Figure 3.6 SEM image of hydrogel coated sample...……...……20

Figure 3.7 Hydrogel coated sample heat flux as a function of resistance……21

LIST OF TABLES

Table 2.1: glass fiber membrane data sheet……6

ACKNOWLEDGEMENTS

I would like to acknowledge Professor Renkun Chen for his support as the chair of my committee. Through two years of study, his guidance has proved to be invaluable.

I would also like to acknowledge members of TEMP. Especially, Aditi Kalle's help with experiments; Qingyang Wang's help with the experimental setup; Wonjae Jeon's help with degassing setup and Pt sputtering; Yu Pei's help with all the SEM images and Pt sputtering; Tianshi Feng's help with hydrogel permeability test; Jian Zeng's help with hydrogel synthesis.

Chapter 2, in part, is currently being prepared for submission for publication of the material. Haowen Zhang; Aditi Kalle; Wonjae Jeon;Yu Pei; Renkun Chen. The thesis author was the primary investigator and author of this material.

ABSTRACT OF THE THESIS

Scalable thin film evaporator using capillary and osmotic pressure

by

Haowen Zhang

Master of Science in Engineering Sciences (Mechanical engineering)

University of California San Diego, 2023

Professor Renkun Chen, Chair

Heat pipes are widely used in electronic system cooling as they offer benefits with simple structure and high cooling efficiency. With the emergence of new-generation computers disssipating heat fluxes of up to thousands of watts per square centimeter, there is an urgent need to explore innovative heat transfer solutions to meet these higher thermal demands. One promising approach is to improve thermofluidic transport performance of wick structures in heat pipes. However, there is a trade-off between high capillary pressure and high permeability in a wick structure. Here, a low-cost glass fiber-based wicking structure

was presented to enable liquid film evaporation for enhancing both heat transfer coefficient (HTC) and critical heat flux(CHF). The membrane utilized in our study features a biporous structure created by random stacking of glass microfibers. This specific structure was chosen due to its simple and yet advantageous characteristics, allowing for enhanced performance in our capillary-driven wicking structure. A study on the dependence of heat transfer performance on the pore size of glass fiber membranes was conducted. Remarkably, a high CHF up to 600W/cm^2 was observed under the atmospheric pressure with large and equal heater and evaporation area (0.5 cm^2). This indicates that the exceptional ability of the wicking structure to handle high heat fluxes. Additionally, the study revealed that the highest HTC reached a high value of 5.5W/cm^2 K, demonstrating the efficient heat transfer capability of the glass fiber-based wicking structures.

Another potential solution to the trade-off between high capillary pressure and high permeability is to replace the capillary pressure with osmotic pressure using an ionic material such as hydrogel. To demonstrate the feasibility of an osmotically-driven wick, we made two kinds of hydrogel: PSA [poly(sodium acrylate)] and PEGDA[poly(ethylene glycol) diacrylate] and then tested the permeability. Based on the obtained results, we proceeded to calculate the evaporation heat flux theoretically, considering the hydrogel thickness as a variable. Through this analysis, we were able to demonstrate the feasibility of the osmotic pumping wick concept. We also attempted to make some hydrogel-coated samples for the evaporation test.

CHAPTER 1: INTRODUCTION

The advancement of electronic devices has led to an increased demand for efficient heat transfer solutions on main boards to mitigate the risk of high-temperature damage. These heat transfer devices must effectively dissipate high heat fluxes within limited areas while maintaining low temperatures around the main board. Currently, heat pipes have emerged as the most effective cooling devices for mainboards, primarily due to their simple structure and high cooling efficiency. Heat pipes are capable of transferring heat efficiently by utilizing the principles of phase change and thermodynamics. They consist of a sealed tube with an inner wick structure and a working fluid. When heat is applied to one end of the heat pipe, the working fluid vaporizes and travels to the cooler end, where it condenses and releases heat. The condensed fluid then returns to the heated end through capillary action within the wick structure, ensuring a continuous cycle of heat transfer. One of the key advantages of heat pipes is their versatility in size. They can be manufactured in compact dimensions, making them suitable for cooling CPUs on small mainboards. However, it is important to note that the average heat flux capacity of conventional heat pipes typically ranges from tens to hundreds of watts per square centimeter. With the emergence of new-generation computers generating heat fluxes of up to thousands of watts per square centimeter, there is a need to explore innovative heat transfer solutions to meet these higher thermal demands. Engineers have been actively exploring methods to enhance the efficiency of heat pipes, and one promising approach is to improve the fluid transport performance of the wick structure. The wick structure plays a critical role in the operation of a heat pipe as it serves as the evaporator section. Located at the hot side of the heat pipe, the wick structure facilitates the absorption of heat by the working fluid and its

transformation into vapor, effectively removing heat from the hot side. The primary function of the wick structure is to transport the working fluid from the cold side back to the hot side using capillary pumping. To achieve this, the wick structure must exhibit excellent fluid transportation performance. It should efficiently transport the working fluid, ensuring a continuous flow from the cold end to the hot end of the heat pipe. This capillary action is crucial for maintaining the functionality and heat transfer capabilities of the heat pipe. Furthermore, the wick structure also plays a role in transferring heat to the working fluid. It should possess high heat conductance, allowing for efficient heat transfer from the surrounding components or source to the working fluid. This ensures effective heat dissipation and helps maintain optimal operating temperatures within the heat pipe system. By improving the fluid transport performance and heat conductance of the wick structure, engineers can enhance the overall efficiency and heat transfer capabilities of heat pipes, enabling them to handle higher heat fluxes and better meet the thermal demands of advanced applications.

To improve wick fluid transportation, a key principle is to make a good compromise between high capillary pressure and high permeability. The traditional way of making wicks is using sintered copper particles: copper has great heat conductance, and pores between particles can provide capillary pressure. However, there is a trade-off between capillary pressure and permeability: small pores can provide high capillary pressure but have low permeability. Because of this, simply decreasing pore size to get high capillary pressure is not a good option. To optimize the fluid transport performance inside wicks, scientists tested different pore sizes inside the wick, wick thickness, and special wick structures like biporous structures. Semenic and Catton[1] made biporous wicks with different thicknesses, the best thick biporous wick tested had CHF(critical heat flux) at 990 W/cm^2 (147℃ superheat). Egbo et al.[2] fabricated

using sintered-copper particles with 30–200 μm spherical particles. The results show that 60 μm particles result in the minimal wick superheat at $q < 100$ W/cm^2 for 1 and 2 layers of the wick, while the 100/200 μm particles with 3 layers lead to the maximum heat flux of 223 W/cm^2. Weibel et al.[3] also tested sintered powder wicks with different thicknesses and particle sizes, their experiment showed that nanoporous sintered wicks are able to support local heat fluxes of greater than 500 W/cm^2 without the occurrence of dry-out.

Other than traditional sintered copper particles wick, Dai et al.[4] designed an entirely new structure: bonded micro membranes on top of microchannels. This structure decoupled capillary pressure and flow resistance by separating them into two directions. Working fluid flowing in high permeability microchannels axially, micro membranes on top of microchannels providing high capillary pressure in the radial direction using small pore size. With this new direction, people did lots of related research. Some of them focus on optimizing microchannels. For example, Coso et al.[5] developed biporous media consisting of microscale pin fins separated by microchannels, which can dissipate heat fluxes of 277.0 W/cm^2 by wicks with heaters of area 1 cm^2. Cai et al.[6][7] used carbon nanotube(CNT) cluster as a wick structure. Experimental results demonstrate 600 W/cm^2 heat transfer capacity and good thermal and mass transport characteristics in the nanolevel porous media. Others looked into micro membranes: Ryu et al.[8] proposed a nanostructured metal foam, which can incorporate onto the micro post evaporator wicks to enhance the capillary performance. Except for these delicate and expensive nanostructures, some scientists trying to develop a practical wick structure, Wena et al.[9] present a cost-effective hybrid wick structure using commercial copper micro meshes along with simple etching processes. Enhanced CHF (198.6 W/cm^2) and HTC (138.7 kW/m^2 K) are observed on this kind of hybrid mesh wick structure. The newest research went to a device-level

test. Hanks et al.[10][11] made not only the wick structure but also the water supply structure feasible for a tiny vapor chamber. Their device-level pure evaporation heat flux reached 144 ± 6 W/cm^2 for water, and the highest evaporation heat flux was obtained with pentane at 550 ± 90 W/cm^2.

An alternative method to enhance the fluid transport capability of wick structures is by utilizing osmotic pressure generated within hydrogels for fluid supply, where suitable hydrogels can be coated on the wick structure to replace capillary pressure with higher osmotic pressure (which can reach tens or hundreds of atmospheres compared to the limited capillary pressure of 1 atmosphere), although the realization of this idea is currently lacking, extensive research exists on heat and mass transfer in hydrogels[12]. Etzold et al.[13] presented experiments and theory relating to transpiration through the hydrogel. Their one-dimensional model shows a relationship between osmotic pressure and transpiration in the hydrogel. However, this relationship is not linear, because Structural changes of water in a hydrogel during dehydration are not linear. As Sekine and Fukazawa[14] mentioned, there are two types of water inside hydrogel: free water and combined water. The first one is easy to leave hydrogel, while the second one is hard to leave for the chemical bond between the water molecule and the hydrogen molecule. In the mathematics model, permeability is another key factor for transpiration through the hydrogel. Decock et al.[15] reported a method to measure PEGDA hydrogel permeability. Their results show Darcy permeability $\kappa \simeq 1.5 \times 10{-}16\ m^2$ for PEGDA hydrogel (using PEG as porogen).

Besides, hydrogel for solar desalination is an active study area, which involves heat and mass transfer in hydrogel[16][17][18].

CHAPTER 2:THIN FILM EVAPORATION ON GLASS FIBER MEMBRANE

2.1 Bi-porous structure enhanced thin film evaporation

Bi-porous means there are two distinguished characteristic pore sizes. This is a common strategy to give wick great water transport performance because small pores can provide high capillary pressure while big pores provide low vapor flow resistance. In this paper, we chose a glass fiber membrane as a wick structure. Figure 2.1 shows the microscopic structure of the glass fiber membrane. It is clear to see two distinguished characteristic pore sizes caused by glass fiber random scattering. Another evidence of a bi-porous structure is this type of membrane has a nominal pore size of around 0.6um as a filter, but from the SEM image, there are lots of porous around 3-20um. With a bi-porous structure, a glass fiber membrane can reach a good compromise between high capillary pressure and high water and vapor permeability.

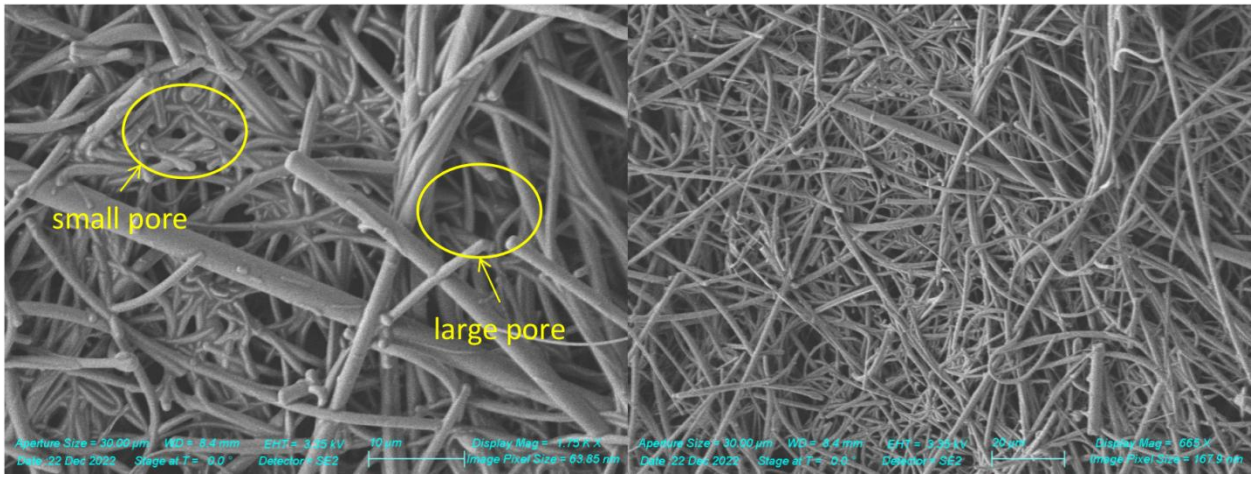

Figure 2.1: SEM image of glass fiber membrane after Pt sputtering

2.2 Sample preparation

Three different types of glass fiber membranes(GA 55, GB 140, grade E) were bought from sterliTECH, the datasheet is shown in Table 2.1. Water flow means: The time in seconds to filter 100 ml of distilled water at 20°C under pressure supplied by a 10 cm water column through a 10 cm² section of the filter, we can calculate permeability from it. TMSPMA and acetic acid were bought from Sigma-Aldrich.

Table 2.1: glass fiber membrane datasheet

Name	Nominal pore size(um)	Water flow(s)	Permeability(m^2)	Thickness(mm)	Price ($)
GB-140	0.4	58	8.59E-13	0.56	0.40
GA-55	0.6	23	8.13E-13	0.21	0.25
Grade E	1.5	12	2.59E-12	0.35	0.15

Sample preparation steps went as follows: Immersed glass fiber membrane inside silane solution(50 ml DI water, 2 µl of acetic acid with pH 3.5, and 1 ml of TMSPMA)[16] and rest at room temperature for two days. A 7mm wide, 250nm thick strip of platinum(Pt) was deposited on each sample, the strip was shaped by hand made tape mask. This Pt layer worked as a resistive temperature detector (RTD) and heater. Then applied silver paste on two sides of the strip as contact pads, leaving a 7*7mm central area as the working area. Heating sample up to 100 degrees C for 15 minutes to cure the silver paste.

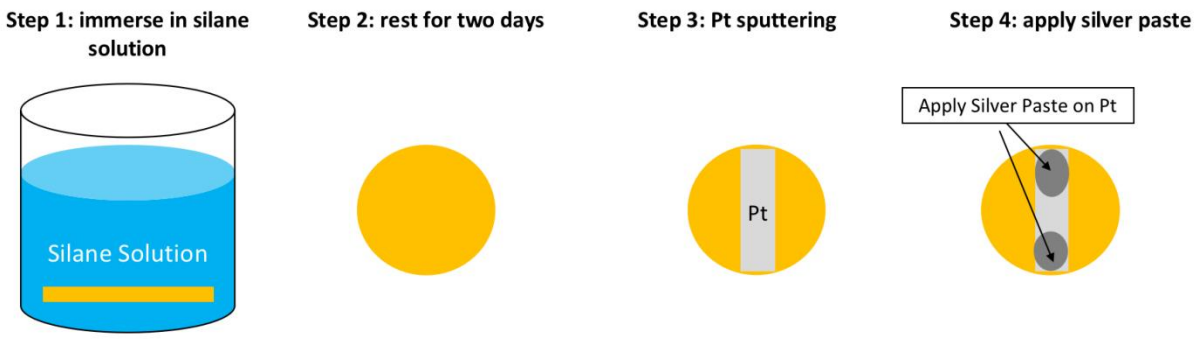

Figure 2.2: schematics of the sample preparation procedure

Silane solution works as a coupling agent, making adhesion between glass fibers and securing their junctions. The steady of glass fiber junctions is extremely important for Pt heater because the Pt heater depends on junctions to form a continuous layer. If some junction disconnected during evaporation, the Pt layer does not continue anymore, thus causing heater failure.

The Pt layer deposited on top of the membrane served as both the heater and RTD in this experiment. The resistance of the heater is around 3ohm. During the experiment, the heater was connected to a power supply, generating hundreds of watts of heat for the evaporation test. The temperature coefficient of resistivity (TCR) of the Pt layer was calibrated for three samples and used the averaged value to get the Pt layer temperature during the evaporation test. After Pt deposition, a K-type thermal couple was attached to the center area of the Pt layer, and thermal glue was used for good heat conduction. After 24 hours of thermal glue curing, applied silver paste and connect copper foil on two sides of the Pt heater for resistance measurement. Heated sample to 100 degrees C for 15 minutes to cure silver paste, then attached sample to a hot plate. The resistance and temperature were recorded simultaneously. Figure 2.3 shows an example of Pt layer calibration. The resistance of the heater shows a good linear relationship with temperature.

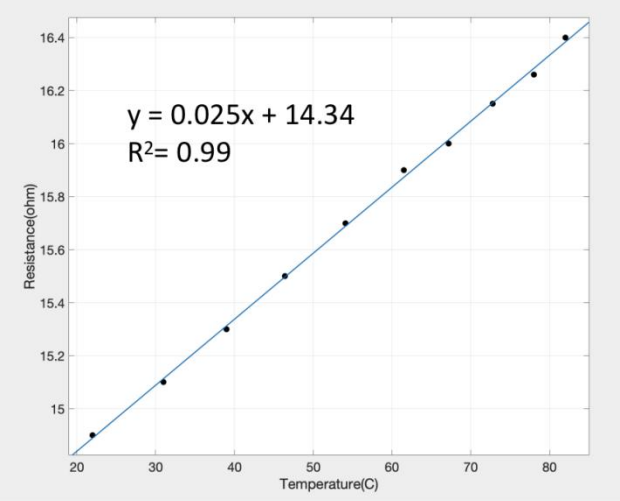

Figure 2.3: TCR calibration curve of the Pt layer

2.3 Experimental Setup and Procedure

As shown in Figure 2.5, the experimental setup consists of two parts: evaporation setup and degassing chamber. The evaporation setup (figure 2.4)is the main part of this experiment. Evaporation set up a held sample applied power to the Pt heater on top of the sample, and water to the whole sample. The sample was held by a pair of round PMMA holders with a 0.7 × 0.7 cm^2 (0.5 cm^2) square hole. In order not to damage the fragile sample, we put a pair of homemade silicone gaskets between the sample and the PMMA holder. We purchased solutions from Mc master, followed the recipe to mix them and drop them into PMMA mold, and incubated them in the air for 24 hours to get silicone gaskets. The heating power was applied to the sample through an alternating current (AC) transformer to the Pt heater. Transformer was connected to the Pt heater and deposited on the sample using copper foil. We put a layer of Sn foil between the copper foil and silver paste contact pads for better connection. Holders together with sample and metal foil were assembled onto a custom-made liquid supply channel using screws and O-ring sealing. Screws also provided mechanical force for the connection between the metal foil and

contact pads. The whole evaporation setup was on an adjustable table, so we can control the water level by adjusting the table height.

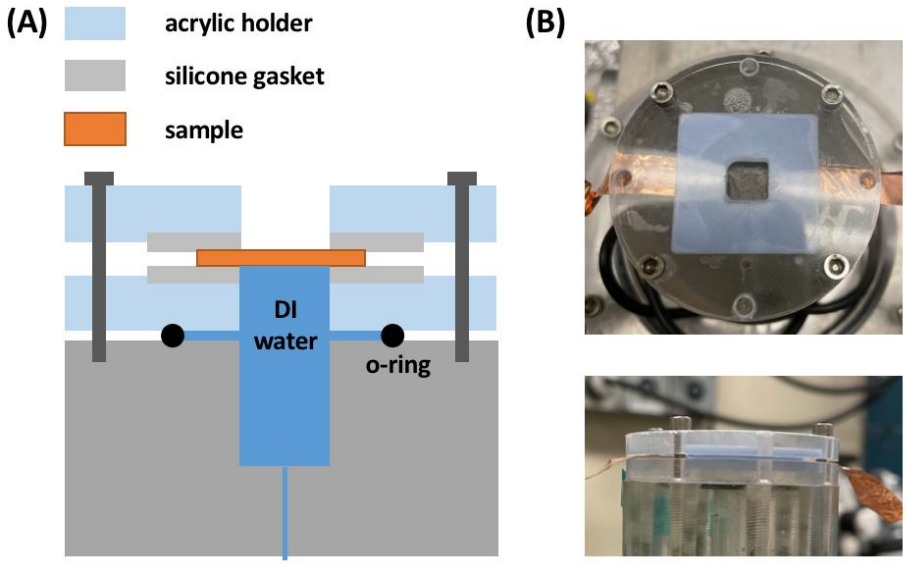

Figure 2.4 Schematic and photos of evaporation setup. (A)schematic of evaporation setup. (B) top view and side view photo of evaporation setup

Water came from the water reservoir inside the degassing chamber, water flow was driven by hydraulic pressure in a water reservoir. DI water was degassed in the degassing chamber by boiling at low pressure(90 kPa) for 5 minutes. After degassing, we heated water up to 100 ℃, so the pressure inside degassing chamber came to 1atm, and degassed water could flow to the evaporation setup. Heat water up to 100 ℃ can also prevent air resolution when we conducted experiments in the open air. To transport hot water, we used Extreme-Temperature PTFE Semi-Clear Tubing and Hot Drinking Water Push-to-Connect Fitting purchased from Mc master.

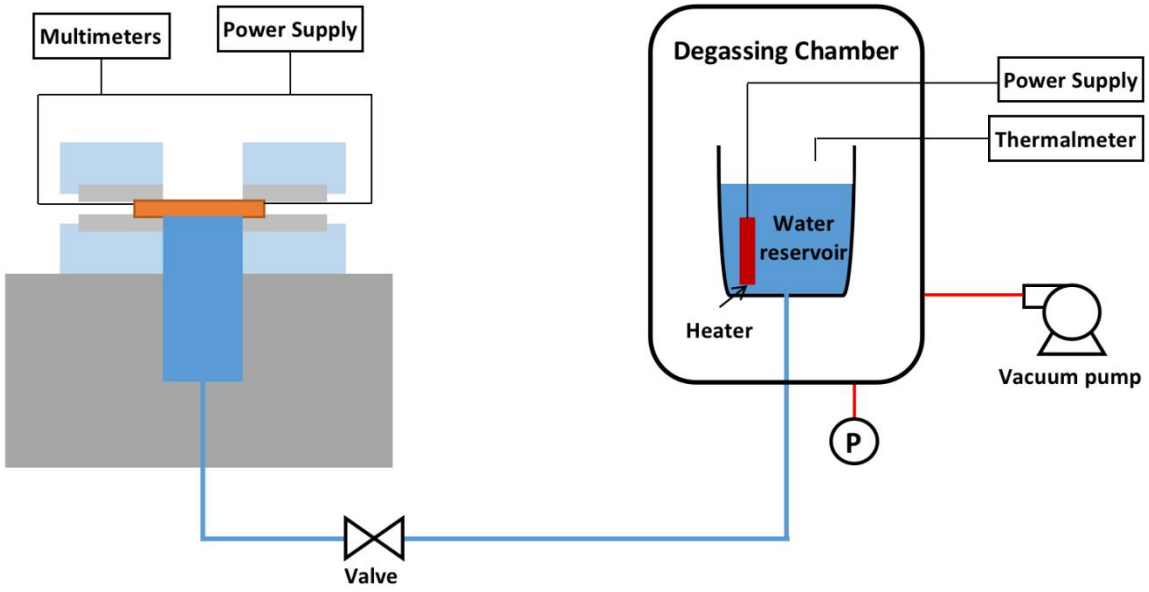

Figure 2.5 Schematic of the experimental setup

The circuit diagram is shown in Figure 2.6. We were dealing with a pretty high current up to 7A, which exceeded the multi meter's up limit. To solve this problem, we put a small resistor(3.75mohm) in series, measured the voltage drop over this resistor, and calculated the current using Ohm's law. Meanwhile, there was another multimeter measuring voltage drop over the testing sample. With the sample's voltage and current, we calculated its heating power and resistance. The resistance can be converted to temperature using TCR. Thus we can plot heat flux as a function of temperature.

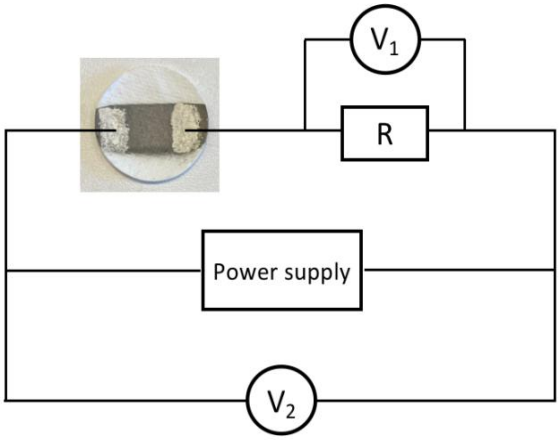

Figure 2.6 Circuit diagram of the evaporation setup

To get the current measuring error, we used current and voltage readings from the power supply to calibrate the shunt resistor. The way getting current from the shunt resistor is measuring the voltage drop over the resistor using multimeter, then divided resistor's resistance 3.75mohm. We measured the current using power supply reading and shunt resistor at the same time and compared the result. The error between these two groups of data was lower than 1%, which is acceptable.

Experimental procedure goes as follows: first check if all the pipes are connected correctly, then close the water feed valve. The degassing process was then initiated, which involved pressure reduction and thermal regulation. A stainless-steel bucket was prepared with a heater placed inside. Deionized (DI) water was filled in the bucket, which was sealed with a lid. A thermocouple was attached to the lid to measure the temperature of the steam, and a thermometer was used to read the temperature from the thermocouple. To contain the steam, the lid was covered with aluminum foil. For pressure reduction, after the degassing chamber was closed, the pressure pump was switched on. The degassing chamber was allowed to reach the minimum pressure(typically around 90 kPa) to create a vacuum. Once the degassing chamber

reached the desired maximum pressure, the pressure pump was switched off. The following is thermal regulation. To regulate the temperature, the heater in the bucket is connected to the power supply, and the heating power is set to a specific value of 600 W, heating the DI water inside the degassing chamber. The DI water is gradually heated until it reaches a temperature of approximately 100°C. Throughout the heating process, the temperature of the steam is monitored and recorded using a thermometer for accurate measurements. The power supply was turned off when the steam temperature reached around 103°C. After degassing, the water transport and sample assembly steps were carried out. Initially, the valve of the liquid feedthrough was opened to allow water flow. The transport of water in the vapor chamber was confirmed by lowering the table and flooding the top of the vapor chamber with water. Subsequently, the liquid feedthrough valve was closed, and the sample, along with the acrylic holder, was placed on top of the vapor chamber. The assembly was completed by adding Cu pads, Indium, and the second acrylic holder, with the silicone portion enclosing the sample. The holders were securely screwed to the vapor chamber, ensuring that all four screws were at the same level. To prevent damage to the sample membrane, a small gap was maintained between the lower acrylic holder and the vapor chamber. Once the assembly was in place, the liquid feedthrough valve was opened again, and the height of the table was increased to the desired level. The consistent flooding of a thin water layer on top of the vapor chamber confirmed the successful establishment of water connection. Then the table level was increased until no visible water layer on top of the sample membrane. With the water transport and sample assembly completed, it is ready for the evaporation test. To measure the current and voltage values, digital multimeters were connected to the sample using alligator clip wires, with the wires also linked to the power supply. Incremental power generation was achieved by employing an amplifier, with power being increased in increments of 5W. The

corresponding voltage and current values were recorded for each increment until the maximum values for current and voltage were obtained. To calculate the critical heat flux (CHF) for the evaporation test, the product of the current and voltage was divided by the heater area.

2.4 Results and Discussion

Figure 2.8 shows evaporation test results of heat flux as a function of temperature. There are three curves, which represented three types of glass fiber membranes. The highest CHF we got is 600W/cm^2 from GB-140. When the evaporation test began, the heater was heated from room temperature, and evaporation enhanced as temperature increased. The gradient on the curve starts to increase when heat flux reached around 20W/cm^2 and keeps increasing until 100W/cm^2, which physically represents the change of the evaporating menisci. The menisci profiles start to vary and the contact angle of the menisci starts to decrease resulting in an increase of the evaporating thin film regions.[1] The menisci keep changing and reach a steady state at around 100W/cm^2 , the gradient thus stays the same until the sample reaches CHF. The CHF and wall superheat have no clear relationship with pore size and thickness. It is probably because CHF is limited by something else other than capillary pressure vs flow resistance in the membrane. The limitation might be local hot spots, thermal stress, and other common problems in high heat flux phase change areas. Unfortunately, we are unable to find the exact limitation in our experiment for now.

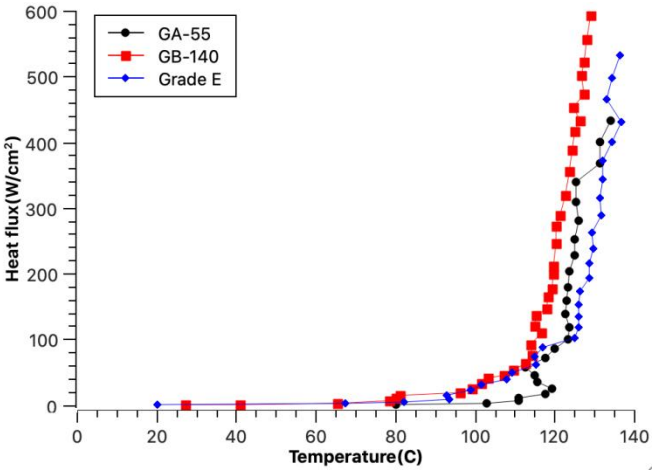

Figure 2.7 Heat flux as a function of temperature of 3 samples

We also calculated the effective heat transfer coefficient using the formula as follows

$$HTC = \frac{q}{(T_{wick} - T_{env})}$$

q is the heat flux, T_{wick} is the sample temperature, T_{env} is the environment temperature. HTC as a function of heat flux is shown in Figure 2.9. The highest HTC is up to 5.5W/cm^2 K, and also has no clear relationship with pore size and thickness.

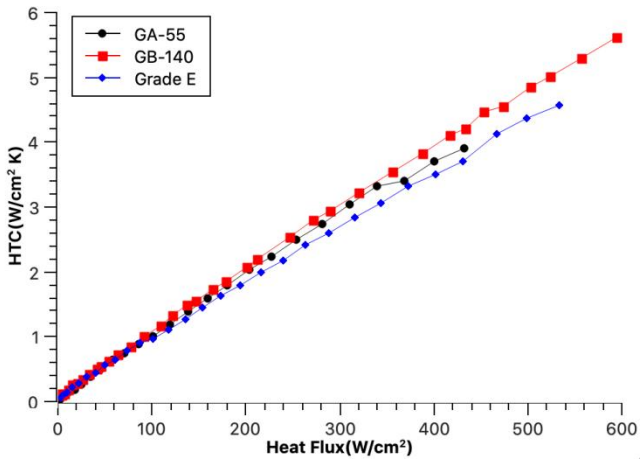

Figure 2.8 Effective heat transfer coefficient as a function of heat flux

Chapter 2, in part, is currently being prepared for submission for publication of the material. Haowen Zhang; Aditi Kalle; Wonjae Jeon;Yu Pei; Renkun Chen. The thesis author was the primary investigator and author of this material.

CHAPTER 3:FEASIBILITY OF USING HYDROGEL IN EVAPORATOR WICK

3.1 Synthesis of hydrogel

In this paper, we mainly use two types of hydrogels: PSA [poly(sodium acrylate)] and PEGDA[poly(ethylene glycol) diacrylate]. PSA has high osmotic pressure around 90atm[17], but has low permeability. PEGDA hydrogel has high permeability using PEG as porogen[11], but has low osmotic pressure.

For PSA synthesis, we use sodium acrylate (SA, 99%) as a monomer, α-ketoglutaric acid as a photoinitiator, and N, N'-methylenebisacrylamide (MBA, 99%) as a cross-linker. Those chemicals were purchased from Sigma-Aldrich and used as received. SA, MBA, and α acid were dissolved in DI water with a fixed molar ratio of 50:1:1 to obtain a 20 wt% homogeneous solution.

For PEGDA hydrogel synthesis, we use poly(ethylene glycol) diacrylate(PEGDA, average Mn 700, 99%) as a monomer, as photoinitiator, poly(ethylene glycol)(PEG, average Mn 8000, 99%) as porogen. Those chemicals were purchased from Sigma-Aldrich and used as received. PEGDA, PEG, and initiator were dissolved in DI water with a fixed molar ratio of

To control the thickness of hydrogel, we made a mold using two glass planes and a 1.5mm thick rubber spacer. The Hydrogel solution was moved to a glass mold by dropper, then applied UV light for 5 minutes. We took hydrogel out from mold and immersed it in DI water overnight to remove unreacted chemicals.

3.2 Permeability test on hydrogel

In order to theoretically calculate the mass flow rate through the hydrogel, we designed an experiment to test the hydrogel's permeability. Permeability k (m^2) in Darcy's law has the definition as follows:

$$k = \frac{v\mu\Delta x}{\Delta P}$$

v is the fluid velocity through the porous medium (m/s), μ is the dynamic viscosity of the fluid (Pa*s), so ΔP is the applied pressure difference(Pa), Δx is the thickness of medium(m). According to this formula, we applied pressure around 1atm on hydrogel, gathered water flowed through hydrogel for 1 hour to calculate v, μ which is known from the water property, hydrogel thickness was controlled by glass mold mentioned before.

The schematic and photo of the experiment set up shown in Figure 3.1. The experiment setup consists of a soft tube, hydrogel, hydrogel holder, iron support, bike pump, and beaker. Soft tube act as a water reservoir and also provided a little hydraulic pressure. Hydrogel was sealed in a hydrogel holder with epoxy. There was a steel mesh under the hydrogel preventing it dropped out from the holder. The Hydrogel holder and soft tube were connected by an o-ring and clamp. To conduct the experiment, we took a piece of fully saturated hydrogel, swipe water on the surface using tissue, then sealed it on a hydrogel holder together with steel mesh. The epoxy took 1 hour to cure. The hydrogel holder was then connected to a soft tube, and some water was added into the soft tube, the water level inside the tube was around 26-30cm. The other side of the soft tube was connected to the bike pump, we pushed the pump until the pressure read 1atm. With this pressure, water flowed through the hydrogel and dropped into a beaker placed under a hydrogel holder. After 1 hour, we measured the amount of water inside the beaker and used it to calculate the hydrogel's permeability.

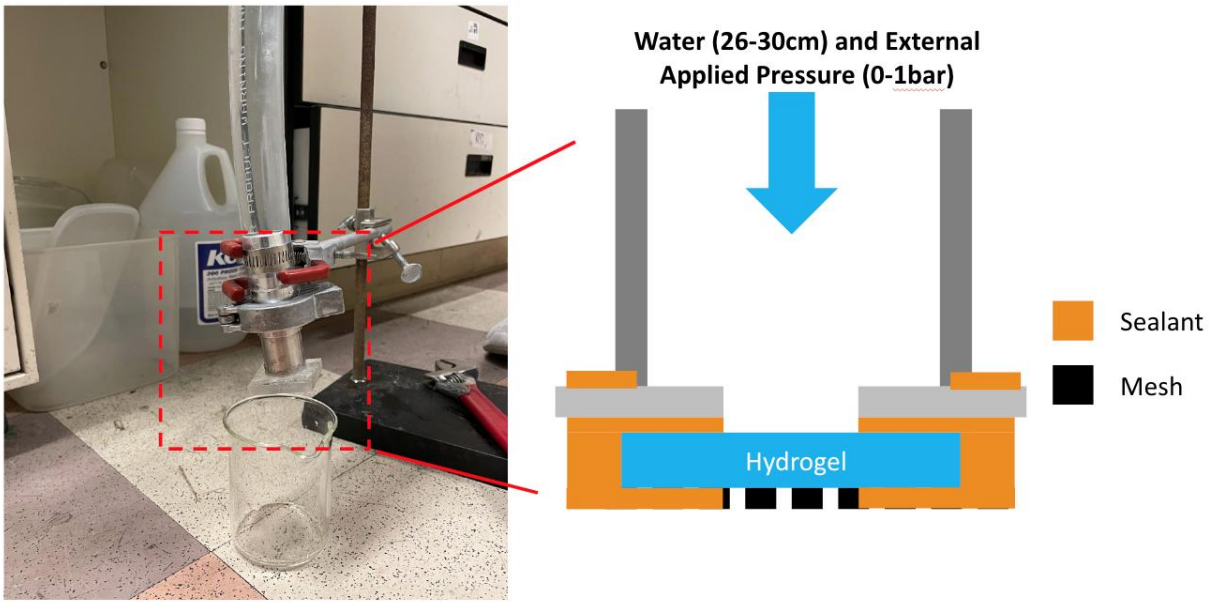

Figure 3.1 Schematic and photo of permeability setup

We tested PEGDA hydrogel has a permeability of around 1e-15 m^2. This result is 8 times larger than Jérémy Decock et.al [11]got, probably because our porogen PGE mean molecular weight was 8 times larger than theirs. PSA hydrogel has permeability around 1e-18 m^2. With these data, we can calculate liquid flux in the hydrogel.

3.3 Theoretical calculation about evaporation flux in hydrogel

Our problem can be simplified as this: there is a piece of hydrogel with a certain thickness, its underside is fully in contact with water, and its top surface is heated by a heater. In this situation, the water turns into vapor and leaves from the hydrogel's top surface, moving heat away. In order to transform this problem into a very simplified model, the first step is separating it into two parts: a model that describes water transport from the underside to the topside inside hydrogel, and another model for water evaporation on hydrogel topside.

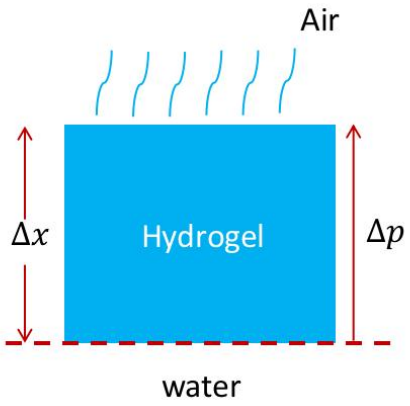

Figure 3.2 Schematic of hydrogel evaporation problem

For the first part, the best mathematical model that can describe water transport inside hydrogel is still controversial in the academic circle. There are some scientists studied similar problems [12][13][20][21]. We choose Darcy's law to describe water transport inside the hydrogel. Darcy's law goes as follows:

$$q = \frac{k\Delta P}{\mu \Delta x}$$

As for hydrogel, q is the fluid velocity through the hydrogel (m/s), k is the permeability of hydrogel(m^2), μ is the dynamic viscosity of water 8.9E-4Pa*s, ΔP is the pressure difference through hydrogel(Pa), Δx is the thickness of hydrogel(m). Permeability is measured as mentioned above: PEGDA hydrogel has a permeability of around 1e-15 m^2; PSA hydrogel has a permeability of around 1e-18 m^2. For pressure difference through the hydrogel, we assume there is a water content gradient over the hydrogel. That means at the underside, hydrogel water content is near 100%, so the osmotic pressure is small enough to neglect; at topside hydrogel, most water is evaporated, so the osmotic pressure is the highest value that the hydrogel can get. Thus, the pressure difference ΔP should be hydrogel's osmotic pressure. We got osmotic pressure of PEGDA[poly(ethylene glycol) diacrylate] and PSA[poly(sodium acrylate)] from

literature: osmotic pressure for 20wt% PEGDA is 9atm[22], osmotic pressure for 20wt% PSA is 230atm[16]. According to Darcy's law, with the value of permeability and pressure difference, we can get mass flux through hydrogel as a function of hydrogel thickness.

For the second model, we simply use latent heat to convert mass flux to heat flux:

$$Q = h\rho q$$

where Q is heat flux, h is the latent heat of water under 1atm 2257 kJ/kg, ρ is water density 1000 kg/m^3, q is the fluid velocity through the hydrogel (m/s). Thus, we get evaporation heat flux as a function of hydrogel thickness.

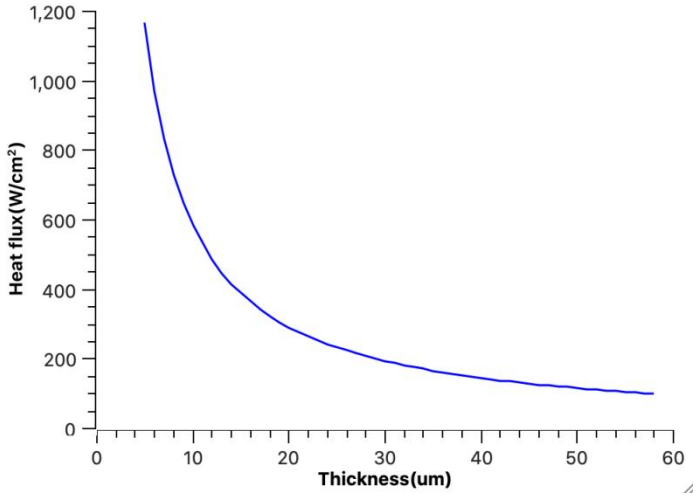

Figure 3.3 PSA max heat flux as a function of thickness

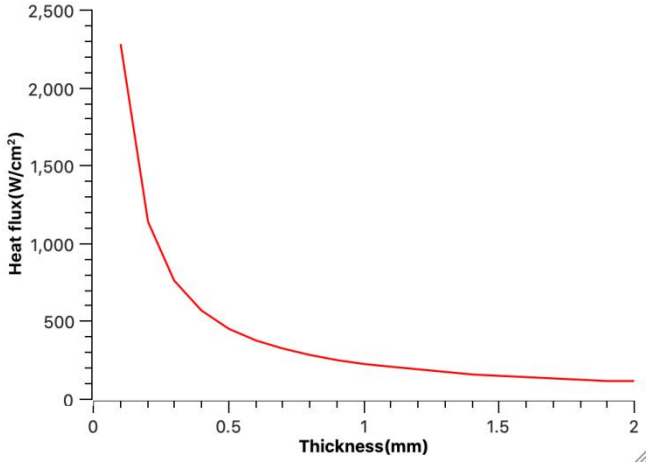

Figure 3.4 PEGDA max heat flux as a function of thickness

For PSA, because of the low permeability, if we can do several micron thick hydrogel coating the heat flux can be up to thousands. For PEGDA, although it has low osmotic pressure, benefits from high permeability hundreds of micron thick coatings can have 1000s W/cm^2 of heat flux. In conclusion, it is possible using hydrogel as an evaporator material theoretically. To make hydrogel with better performance, one key point is to increase its permeability.

3.4 Evaporator with hydrogel

After theoretically proving the feasibility of using hydrogel in the evaporator wick, we made some evaporators with PEGDA hydrogel. We choose the glass fiber membrane mentioned above as substrate, using silane solution to modify the surface for hydrogel coating. For the coating procedure, we first put 1ml 20%vt PEGDA solution on the membrane, then put it under UV light for 10s to synthesize. However, this type of sample burned at 20W/cm^2 during the evaporation test. We guess the problem might be the thickness of the hydrogel. Therefore, we introduced spinning coating to reduce hydrogel coating thickness. In the whole procedure shown in Figure 3.5, we did spin coating under 1500rpm for the 50s.

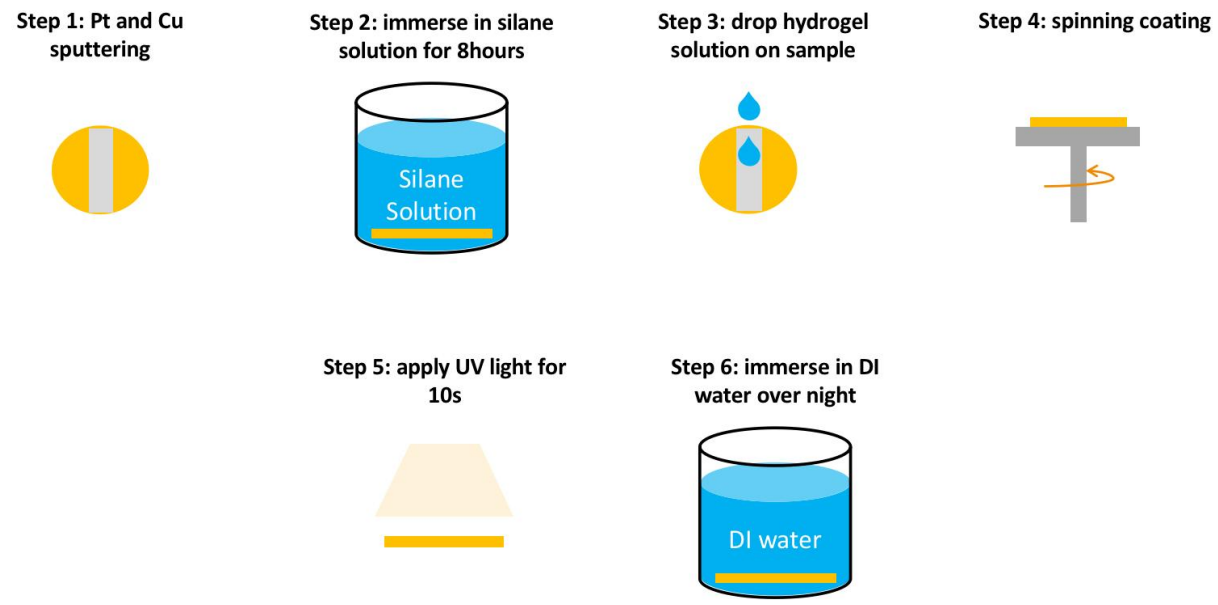

Figure 3.5 Procedure of making hydrogel coated evaporator

Figure 3.6 shows the SEM image after hydrogel coating. From the picture on the left, we can see the sample has a very thin hydrogel coating between the glass fiber, meanwhile, some small pores remained open. The size of these small pores is around several micros. However, more than half of the pores are still blocked by hydrogel as shown in the right picture.

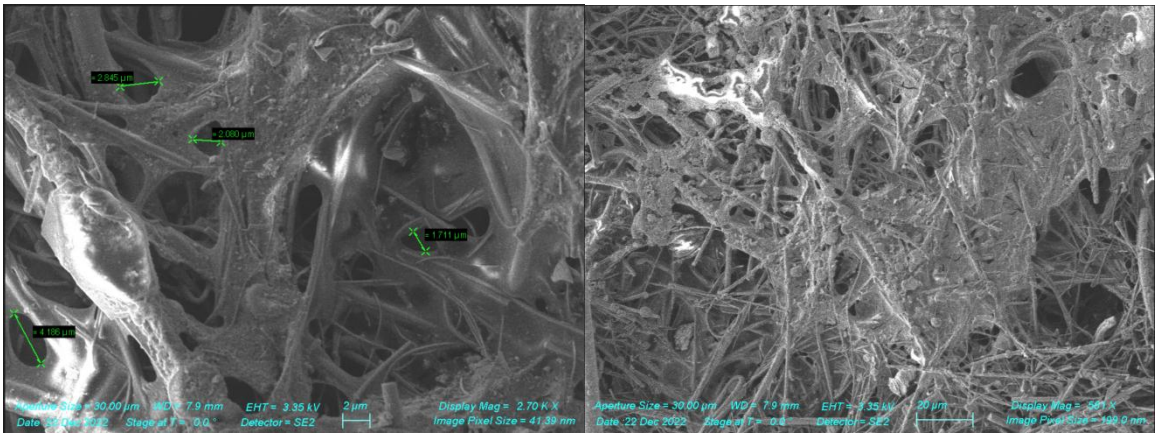

Figure 3.6 SEM image of hydrogel coated sample

Because of this, the evaporation test result for this kind of sample is only around 120W/cm^2. Another problem is hydrogel coating increases contact resistance between the sample

and copper foil, RTD is influenced by contact resistance so we couldn't get the temperature. For future work we will focus on solving these two problems: optimize the spinning coating procedure and reduce contact resistance.

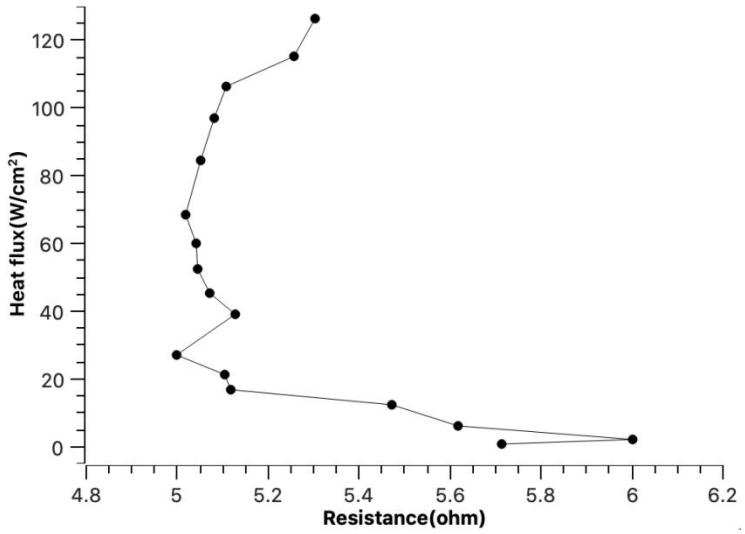

Figure 3.7 Hydrogel coated sample heat flux as a function of resistance

CHAPTER 4:SUMMARY AND FUTURE WORK

4.1 Summary

For the capillary driven wick, a low-cost glass fiber based wicking structure was presented to enable liquid film evaporation for enhancing both CHF and HTC. The membrane utilized in our study features a bio-pores structure created by randomly pressing glass fibers together. This specific structure was chosen due to its simple but advantageous characteristics, allowing for enhanced performance in our capillary-driven wicking structure. A study on the dependence of heat transfer performance on the pore size of glass fiber membranes was conducted. Remarkably, a high CHF of 600W/cm^2 was observed under atmosphere pressure when the heater area and evaporation area were equal (0.5cm^2). This indicates the wicking structure's exceptional ability to handle high heat fluxes. Additionally, the study revealed that the highest HTC reached an impressive value of 5.5W/cm^2 K, demonstrating the efficient heat transfer capability of the glass fiber-based wicking structure.

For the osmotically driven wick, we made two kinds of hydrogel: PSA and PEGDA, then tested the permeability. Based on the obtained results, we proceeded to calculate the evaporation heat flux theoretically, considering the hydrogel thickness as a variable. Through this analysis, we were able to demonstrate the feasibility of the osmotic pumping wick concept. We also attempt to make some hydrogel-coated samples for the evaporation test.

4.2 Future work

In the case of glass fiber membrane, future work involves integrating it into a device alongside suitable microchannels, which should exhibit high thermal conductivity. Copper microchannels, for instance, are a viable choice. It has been demonstrated that glass fiber and

copper microchannels can be consolidated through a sintering step performed at 800°C for approximately 5 minutes [23]. By utilizing this approach, a device incorporating a glass fiber membrane can be fabricated, and device-level results can be obtained. This step is crucial for enhancing overall performance in practical vapor chamber applications.

For osmotic pumping, there is still a lot of work to do. For now, there are mainly three parts to it:

1. Optimization of Hydrogel Coating Procedure:

To further advance the development of osmotic pumping wick structures, the optimization of the hydrogel coating procedure is a primary focus. The coating process should be refined to ensure consistent and uniform coverage of the wick surface with the hydrogel material. Parameters such as coating thickness, deposition method, and drying conditions should be systematically investigated and optimized to achieve the desired performance.

2. Permeability Analysis of Hydrogel-Coated Samples:

To validate the effectiveness of osmotic pumping, it is essential to evaluate the permeability of the hydrogel-coated samples and compare it with that of the bulk hydrogel. This analysis will provide insights into the transport properties of the hydrogel coating and determine if it exhibits similar permeability characteristics to the bulk hydrogel material. Permeability tests or specific characterization methods for hydrogels can be employed to quantify the permeability of the coated samples.

3. Experimental Validation of the Osmotic Pumping Wick Concept:

Experimental validation is crucial to demonstrate the enhanced critical heat flux (CHF) achieved by the hydrogel-coated wick structures through osmotic pumping. By conducting evaporation tests or heat transfer experiments, the performance of the hydrogel-coated samples

can be evaluated and compared with conventional wick structures. The results obtained will provide direct evidence of the osmotic pumping concept and its potential for improving heat transfer performance.

In conclusion, future work includes optimizing the hydrogel coating procedure, evaluating the permeability of hydrogel-coated samples, experimentally validating the osmotic pumping wick concept, and integrating glass fiber membrane with copper microchannels to create a device for obtaining comprehensive performance results. These efforts contribute to the ongoing improvement of heat transfer devices and their practical applications.

REFERENCES

[1] Tadej Semenic, Ivan Catton, Experimental study of biporous wicks for high heat flux applications, International Journal of Heat and Mass Transfer 52 (2009) 5113–5121

[2] Munonyedi Egbo, Yahya Nasersharifi, Gisuk Hwang, Phase-change heat transfer of sintered-particle wick in downward facing orientation: Particle size and wick thickness effects, International Journal of Heat and Mass Transfer 155 (2020) 119840

[3] J. A. Weibel, S. V. Garimella,M. T. North, Characterization of Evaporation and Boiling from Sintered Powder Wicks Fed by Capillary Action, International Journal of Heat and Mass Transfer 53 (2010) 4204–4215

[4] Xianming Dai, Fanghao Yang, Ronggui Yang, Yung-Cheng Lee, Chen Li, Micromembrane-enhanced capillary evaporation, International Journal of Heat and Mass Transfer 64 (2013) 1101–1108

[5] Dusˇan Coso, Vinod Srinivasan, Ming-Chang Lu, Je-Young Chang, Arun Majumdar, Enhanced Heat Transfer in Biporous Wicks in the Thin Liquid Film Evaporation and Boiling Regimes, Journal of Heat Transfer, 2012, Vol. 134 / 101501-1

[6] Qingjun Cai, Chung-Lung Chen, Design and Test of Carbon Nanotube Biwick Structure for High-Heat-Flux Phase Change Heat Transfer, Journal of Heat Transfer, 2010, Vol. 132 / 052403-1

[7] Q. Cai, A. Bhunia, High heat flux phase change on porous carbon nanotube structures, International Journal of Heat and Mass Transfer 55 (2012) 5544–5551

[8] Seunggeol Ryu, Jeonghoon Han, Jichul Kim, Choongyeop Lee, Youngsuk Nam, Enhanced heat transfer using metal foam liquid supply layers for microheat spreaders ,International Journal of Heat and Mass Transfer 108 (2017) 2338–2345

[9] Rongfu Wena, Shanshan Xub, Yung-Cheng Lee, Ronggui Yang, Capillary-driven liquid film boiling heat transfer on hybrid mesh wicking Structures, Nano Energy 51 (2018) 373–382

[10] Daniel F. Hanks, Zhengmao Lu,Jay Sircar, Ikuya Kinefuchi, Kevin R. Bagnall, Todd R. Salamon, Dion S. Antao, Banafsheh Barabadi, and Evelyn N. Wang. High Heat Flux Evaporation of Low Surface Tension Liquids from Nanoporous Membranes, ACS Appl. Mater. Interfaces 2020, 12, 7232−7238

[11] Daniel F. Hanks, Zhengmao Lu, Shankar Narayanan, Kevin R. Bagnall, Rishi Raj, Rong Xiao, Ryan Enright, Evelyn N. Wang, Nanoporous Evaporative Device for Advanced Electronics Thermal Management, 14th IEEE ITHERM Conference

[12] Carlos D. Díaz-Marína, Lenan Zhanga, Bachir El Fil, Zhengmao Lub, Mohammed Alshraha,Jeffrey C. Grossmanb, Evelyn N. Wang, Heat and mass transfer in hygroscopic hydrogels, International Journal of Heat and Mass Transfer 195 (2022) 123103

[13] Merlin A. Etzold, P.F. Linden1 and M. Grae Worster, Transpiration through hydrogels, J. Fluid Mech. (2021), vol. 925, A8

[14] Yurina Sekine and Tomoko Ikeda-Fukazawa, Structural changes of water in a hydrogel during dehydration, J. Chem. Phys. 130, 034501 (2009)

[15] érémy Decock,a Mathias Schlenkb and Jean-Baptiste Salmon, In situ photo-patterning of pressure-resistant hydrogel membranes with controlled permeabilities in PEGDA microfluidic channels, Lab Chip, 2018, 18, 1075

[16] Jian Zeng, Qingyang Wang, Yang Shi, Ping Liu, and Renkun Chen, Osmotic Pumping and Salt Rejection by Polyelectrolyte Hydrogel for Continuous Solar Desalination, Adv. Energy Mater. 2019, 1900552

[17] Fei Zhao, Xingyi Zhou, Ye Shi, Xin Qian, Megan Alexander, Xinpeng Zhao, Samantha Mendez, Ronggui Yang, Liangti Qu and Guihua Yu, Highly efficient solar vapour generation via hierarchically nanostructured gels, Nature Nanotechnology volume 13, pages489–495 (2018)

[18] Youhong Guo, Luize Scalco de Vasconcelos, Neha Manohar, Jiafeng Geng, Keith P. Johnston,and Guihua Yu, Highly Elastic Interconnected Porous Hydrogels through SelfAssembled Templating for Solar Water Purification, Angew. Chem. Int. Ed. 2022, 61, e202114074

[19] Hyunwoo Yuk, Teng Zhang, Shaoting Lin, German Alberto Parada and Xuanhe Zhao, Tough bonding of hydrogels to diverse non-porous surfaces, NATURE MATERIALS, 2016, vol 15

[20] Gavin Hoch, Anuj Chauhan, C.J. Radke, Permeability and diffusivity for water transport through hydrogel membranes, Journal of Membrane Science 214 (2003) 199–209

[21] I. Fatt and Thomas K. Golds tick, DYNAMICS OF WATER TRANS PORT IN S WELLING MEMBRANES, February 9, 1965

[22] Nicholas P. Money, Osmotic Pressure of Aqueous Polyethylene Glycols Relationship between Molecular Weight and Vapor Pressure Deficit, Plant Physiol. (1989) 91, 766-769

[23] Mengnan Jiang, Yang Wang, Fayu Liu, Hanheng Du, Yuchao Li, Huanhuan Zhang,

[24] Suet To, Steven Wang, Chin Pan, Jihong Yu, David Quéré Zuankai Wang, Inhibiting the Leidenfrost effect above 1,000 °C for sustained thermal cooling, Nature,Vol 601,27 January 2022